ISSN 0021-3640, JETP Letters, 2020, Vol. 112, No. 3, pp. 186–192. © Pleiades Publishing, Inc., 2020.
Russian Text © The Author(s), 2020, published in Pis'ma v Zhurnal Eksperimental'noi i Teoreticheskoi Fiziki, 2020, Vol. 112, No. 3, pp. 196–202.

CONDENSED MATTER

Simulation of the Quantum Hall Effect in Samples with Weak Long-Range Disorder[1]

O. A. Tkachenko[a, *], V. A. Tkachenko[a, b], D. G. Baksheev[b], and O. P. Sushkov[c]

[a] *Rzhanov Institute of Semiconductor Physics, Siberian Branch, Russian Academy of Sciences, Novosibirsk, 630090 Russia*

[b] *Novosibirsk State University, Novosibirsk, 630090 Russia*

[c] *School of Physics, University of New South Wales, 2052 Sydney, Australia*

**e-mail: otkach@isp.nsc.ru*

Received June 1, 2020; revised July 3, 2020; accepted July 7, 2020

The fine structure of the density of states is studied numerically in the quantum Hall effect mode during the ballistic transmission of an electron through an area of 1 μm^2 of a two-dimensional electron gas with weak long-range disorder. The calculated widths of strict quantum plateaus agree with experimental data. Periodic conductance oscillations corresponding to the addition of two electrons to the simulated area are found in the central part of the lower Landau band. One-dimensional countercurrents are found inside the area and at its edge, which are separated by a magnetic length and explained by the motion of an electron with a low drift velocity.

DOI: 10.1134/S0021364020150114

The quantum Hall effect (QHE) [1, 2] is well known in context of its relation to world constants and clear experimental manifestations in various two-dimensional conducting systems (see reviews [3–6] and references therein). Despite the vast literature on the QHE mechanism, it remains unclear how the transition occurs between the modes of localized, delocalized, and edge states [3, 7, 8]; whether they coexist; how the widths of the quantized resistance plateaus and transition regions relate to each other; how these widths depend on the type, amplitude of the disorder, and large-scale features of the potential [9–13]; how disorder affects the Landau quantization [3, 4, 14, 15]; and what role the spin, interaction, correlations, and phase transitions play in a multiparticle system in the QHE [4–6, 13, 16, 17]. Many quantum mechanical calculations were performed to explain the QHE, including very complicated ones [16, 17]. In these cases, the results were speculatively extrapolated to macroscopic systems with a two-dimensional electron gas (2DEG), although they were obtained for the submicron simulated region. At such sizes, the contribution of edge states to the widths of quantized plateaus is much larger than that in macrosystems, where the contributions of decoherence [5], compressible/incompressible strips [12], and Hall field inhomogeneities [13] are important. The simulation of the experimental observations of the QHE in small mesoscopic structures would answer some of the questions.

Owing to improved technology and measurements [6, 18–20], it has recently become possible to observe the QHE in a very pure ballistic structure with a 2DEG square with an area of 1 μm^2 and rather sharp edges (with almost no incompressible strips) [21]. It is important that the Hall plateaus are observed in small samples not only in the resistance R_{xy} [22, 23] but also in the conductance measured diagonally across the sample G_{xy} [21, 24] and in the conventional two-terminal conductance [25, 26]. The interpretation of the two-terminal conductance within the Landauer approach [27] does not require considering Hall fields and chemical potential distributions within the sample, which is necessary for macrosystems [13].

The aim of this work is to simulate the integer quantum Hall effect in structures with a clean two-dimensional electron gas, while limiting the calculations to the coherent scattering of a particle on weak long-range disorder in square samples with sides from 1 to 4 μm in a two-terminal situation. Disorder is considered long-range if its correlation length $L_{\rm corr}$ is much larger than the magnetic length l_B. A universal method for solving the problem of one-particle quantum scattering is the method of nonequilibrium Green's functions [27, 28], which makes it possible to find numerically the local and total density of states ($LDoS(x, y)$ and DoS), conductance G, and the distri-

[1] Supplementary materials are available for this article at https://doi.org/10.1134/S0021364020150114 and are accessible for authorized users.

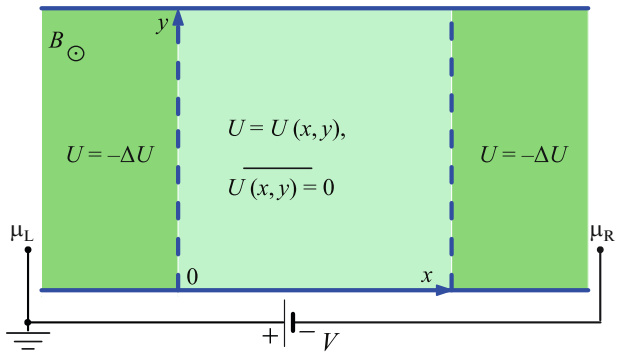

Fig. 1. (Color online) Schematic representation of the simulated situation: the scattering region with the potential $U(x, y)$ is bounded by the dashed lines in the channel, U is the potential in the two-dimensional Schrödinger equation, μ_L and μ_R are chemical potentials, and V is the voltage between reservoirs of the two-dimensional electron gas.

bution of the nonequilibrium current $J(x, y)$ for almost any small two-dimensional system built into a homogeneous channel [29–32]. The two-dimensional effective potential $U(x, y)$ used in this work was obtained by the numerical solution of the three-dimensional electrostatic problem for a solid structure defined by a correlated distribution of localized charges in a plane remote from the 2DEG [33]. Disorder in $U(x, y)$ is characterized by the Gaussian correlation function $\exp[-(|\Delta \mathbf{r}|/L_{corr})^2]$. Calculations show that, depending on the distance z between the plane of localized charges and the 2DEG, the correlation length L_{corr} changes from 30 to 100 nm. At $z \geq 40$ nm ($L_{corr} \geq 80$ nm), the disorder can be considered long-range, $L_{corr} \gg l_B$, in quantizing magnetic fields $B \geq 1$ T ($l_B \leq 26$ nm). The method of calculating $U(x, y)$ and L_{corr} is given in the supplementary materials. To simulate the weakening of disorder, we multiplied the potential $U(x, y)$ by some factor less than one. The ranges of the variation of potential fluctuations (0.05–1.5 meV) and, accordingly, the standard deviations δU_{rms} (0.016 to 0.5 meV) correspond to a high quality of structures (with a mobility of 10^6–10^7 cm^2/(V s)) [6, 18, 20]. In the proposed QHE model, the scattering region is built into a homogeneous channel, where the potential U is assumed to be $-\Delta U$ and infinite at the boundaries (Fig. 1). The channel is located between wide reservoirs with the 2DEG. The distribution functions of electrons incident on the scattering region from the left ($k_x > 0$) and from the right ($k_x < 0$) are $f^+(E) = \Theta(\mu_L - E)$ and $f^-(E) = \Theta(\mu_R - E)$, respectively [27]. The two-terminal conductance is determined by the Landauer formula for zero temperature at $V \to 0$. One-particle states at $V = 0$ are filled up to the Fermi level E_F. The spin splitting of the states [3, 5] and the dependence of the two-dimensional potential U on B and the density of the 2DEG n [4, 9, 18] are disregarded. We calculate the dependences of DoS, G, and E_F on n at fixed B, rather than vice versa, as that would require the self-consistent calculation of $E_F(B, n)$. Such calculations without additional hypotheses make it possible to obtain the widths of the quantum conductance plateaus, the fine structure of Landau levels, and the distribution of one-dimensional current states. The results are compared to measurements in large and small samples [10, 11, 18, 19, 21, 23]. The fractional features of the conductance [21, 25, 26] remain outside of the proposed model.

Figures 2 and 3 demonstrate the dependences $DoS(n)$, $G(n)$, and $E_F(n)$ calculated according to the algorithm [28] for *one implementation* of the two-dimensional potential U corresponding to a certain working state of the mesoscopic sample. The calculation used the potential $U(x, y)$ with $L_{corr} = 80$ nm, defined on a 1 × 1-μm square and shown in Fig. 4 together with the coordinate dependences of the local density of states and nonequilibrium current. The problem of quantum scattering was solved at a fixed perpendicular magnetic field $B = 2$ T ($\hbar\omega_c = 3.46$ meV) typical of the QHE. The density of states DoS in the scattering region and the two-terminal conductance G were calculated in terms of the Green's function [27], which was varied with a small step of $\sim 10^{-6}$ meV as a function of the electron energy E. The density of the 2DEG $n(E_F)$ in the scattering region was found by summing $DoS(E)$ starting from the state with $DoS = 0$ to the Fermi energy E_F. Then, various quantities were plotted as functions of the gate-controlled density. The analysis of these dependences is the main content of this work, since they are easy to compare to the measurements of electron transport. The details of the calculations, including the calculated energy dependences, are included in the supplementary materials. Unlike the original dependence $DoS(E)$ (Fig. S2 in the supplementary materials), the Landau levels having the width $\Gamma \sim \delta U_{rms} = 0.016$ meV $\ll \hbar\omega_c$ were transformed into wide bands in the dependence $DoS(n)$ at weak smooth disorder, and the gaps between them were sharply narrowed (Fig. 2a). The fine structure of Landau bands is clearly visible. These bands consist of hundreds of narrow DoS peaks, and their height is orders of magnitude lower near the center than that in the tails. We note that the number of DoS peaks increases with the size of the scattering region. In a macroscopic sample, the dependence $DoS(E)$ is averaged and information on the distribution of localized and delocalized states disappears.

In Fig. 2b, narrow dips are seen on the left side of each conductance quantization plateau. Strict plateaus (perfectly flat regions of quantized conductance) are seen around characteristic densities $n = 10 \times 10^{10}$,

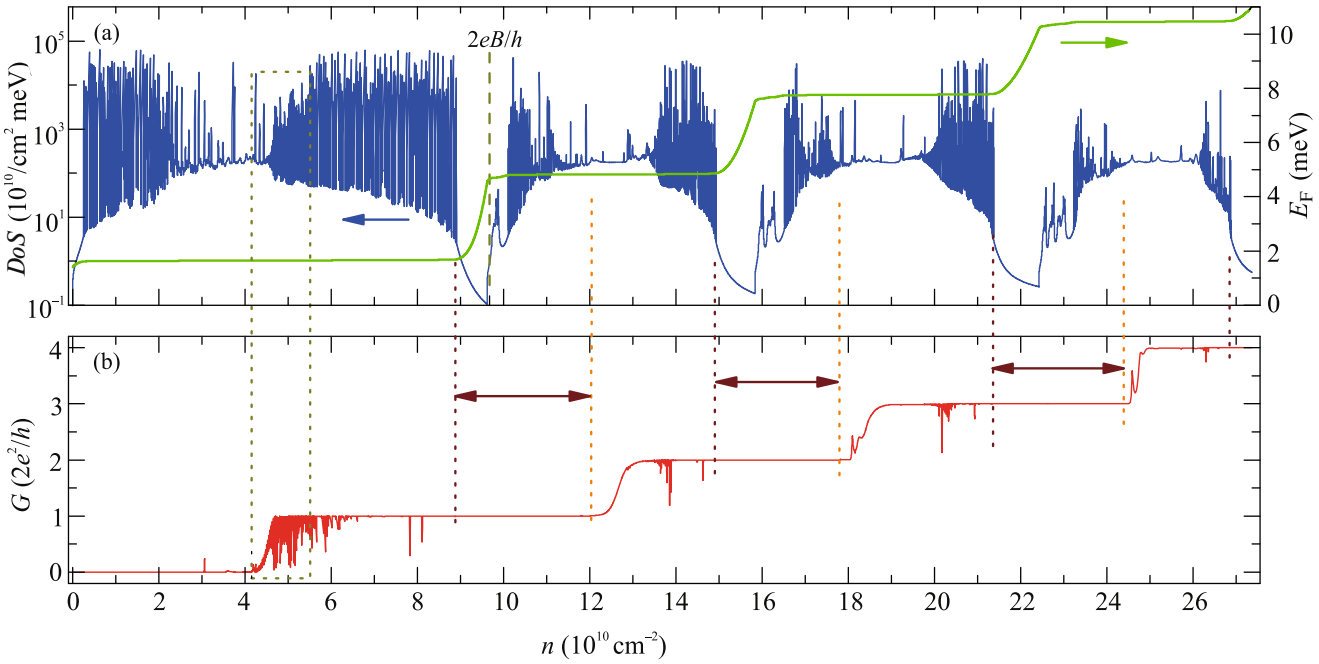

Fig. 2. (Color online) (a, left scale) Density of states $DoS(n)$, (a, right scale) Fermi level $E_F(n)$, and (b) conductance $G(n)$ versus the density of the 2DEG at $B = 2$ T for *one of the implementations* of the potential in the scattering region of 1 μm^2 with $U_{max} - U_{min} = 0.1$ meV, $\delta U_{rms} = 0.016$ meV, $L_{corr} = 80$ nm, and $\Delta U = 0.25$ meV. The horizontal arrows show the widths of the strict quantum conductance plateaus.

16×10^{10}, and 23×10^{10} cm^{-2}, and these regions have the same width. The comparison of the $G(n)$, $DoS(n)$, and $E_F(n)$ plots (Fig. 2) shows that deep dips of DoS and sharp transitions between wide, almost horizontal sections $E_F(n)$ occur near these densities. The strict plateaus penetrate into neighboring Landau bands, while much deeper into the beginning of the higher number bands, so that the centers of the strict plateaus lie along n to the right of the DoS minima, e.g., $2eB/h$. Note that such a shift is rare in experiments, but a shift of the centers of the plateau R_{xy} to higher B was indeed observed under similar conditions [21] compared to those predicted by the classical Hall effect. In Fig. 2, the width of the transition regions $G(n)$, which contain narrow peaks, conductance dips, and gradual changes $G(n)$, is commensurate with the width of the strict plateaus. This is indicated by an approximately equal spacing of 3×10^{10} cm^{-2} between dividing vertical dashed lines (Figs. 2a, 2b). According to Fig. 2, one may expect that the width of strict plateaus in clean structures, taking into account the lifting of spin degeneracy, will be 1.5×10^{10} cm^{-2}. This value *almost coincides* with the measured width of the quantum plateaus at filling factors $\nu = 1$ and 2 in the case of the macroscopic samples with mobilities of $(0.5–4) \times 10^6$ cm^2/(V s) [18]. The fine structure in $DoS(n)$ with a large number of narrow peaks at the edge of the Landau band and its penetration deep into the plateau $R_{xy} = h/2e^2$ are experimentally discovered in the 2 × 13-μm mesoscopic Hall bar [23], which is similar to the behavior at $n \approx 10^{11}$ cm^{-2} in Fig. 2.

Figure 3 zooms into the periodic antiphase oscillations in $DoS(n)$ and $G(n)$ in the central region of the first Landau band. The oscillation period corresponds to the addition of approximately 2.5 electrons to the scattering region, which will be discussed below.

The distributions of the local density of states $LDoS(x, y)$ and current density $J(x, y)$ show the simplest pattern for the dips of DoS, when $E_F - \hbar\omega/2 \gg \delta U_{rms}$ (examples in Figs. 4a, 4b). The usual edge states in the form of narrow lines of increased $LDoS$ at the channel edges are seen, corresponding to the equilibrium current at the zero drift voltage (Fig. 4a). The nonequilibrium current is present only at the edge of the square, which corresponds to a given sign of the difference in the chemical potential in the ideal supply channels. The distribution current over y on this edge appears as a *single* narrow line, and its direction is indicated by an arrow (Fig. 4b). The space outside the specified lines is an insulator, since $LDoS(x, y)$ and $J(x, y)$ here are almost eight orders of magnitude less. Weak smooth disorder in $U(x, y)$ found by solving the three-dimensional electrostatic

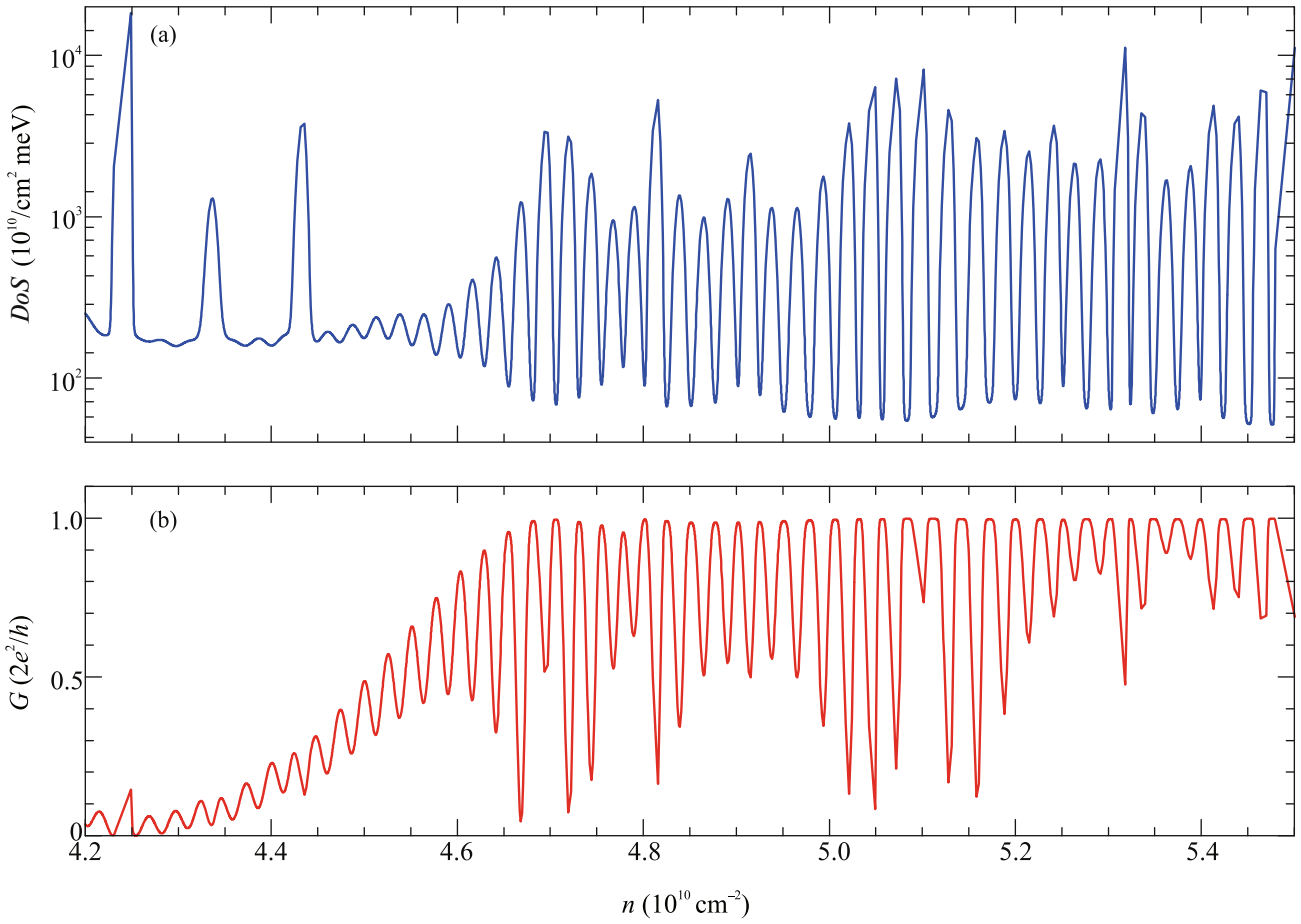

Fig. 3. (Color online) Density of states $DoS(n)$ and $G(n)$ versus the density of the 2DEG corresponding to the region inside the dotted rectangle near the center of the lower Landau band from Fig. 2.

problem (Fig. 4c) does not manifest itself on these lines and in the area of the insulator.

The situation changes qualitatively for states corresponding to the region of periodic oscillations of the conductance near the center of the lower Landau band $E_F - \hbar\omega_c/2 < \delta U_{rms}$. This is shown in Figs. 4d–4f. The comparison with Fig. 4c shows that electrons at the Fermi level fill only the network of *LDoS* lines (Fig. 4e) coinciding with the contours of the potential $U(x, y) = 0$. The widths of curvy lines of $LDoS(x, y)$ are determined by the magnetic length. Between the lines, $LDoS(x, y)$ drops by orders of magnitude. Note that a similar network in *LDoS* was observed experimentally, but for a stronger and less smooth disorder [10]. The nonequilibrium current in Figs. 4d and 4f also flows along the zero-potential contours. Unlike Fig. 4b, it flows in *two opposite* directions, as manifested by the split-line current density J shown with small arrows (the direction of the arrows can be seen at magnification; see the supplementary materials). This effect is explained by the low drift velocity of the electron. In this case, the velocity of circular motion of the electron $\omega_c r_c \approx 10^6$ cm/s is 50 times higher than the drift velocity. It can be seen that *LDoS* is inhomogeneous on the potential contours because of both smooth and abrupt changes in the magnitude and direction of the drift velocity. If electrons with increasing density fill only nondegenerate quasidiscrete levels, then resonances follow with a period corresponding to the addition of two electrons to the entire simulated area. A simple calculation for a Y junction of one-dimensional conductors [29] shows that the average period in n can increase to 2.5 electrons.

In addition to Figs. 4d–4f, Figs. 4g and 4h demonstrate the universality of the effect of electron motion along the $U(x, y) = 0$ contours for the states near the center of the Landau band. In this case, the band is the second one and the conductance is slightly lower than $2 \times 2e^2/h$. Lines of the local density of states are now split (two maxima of probability density). Note that a similar double-peak structure of the curvy *LDoS* lines was recently observed experimentally at less smooth disorder [11]. The J lines in Fig. 4h, as well as in

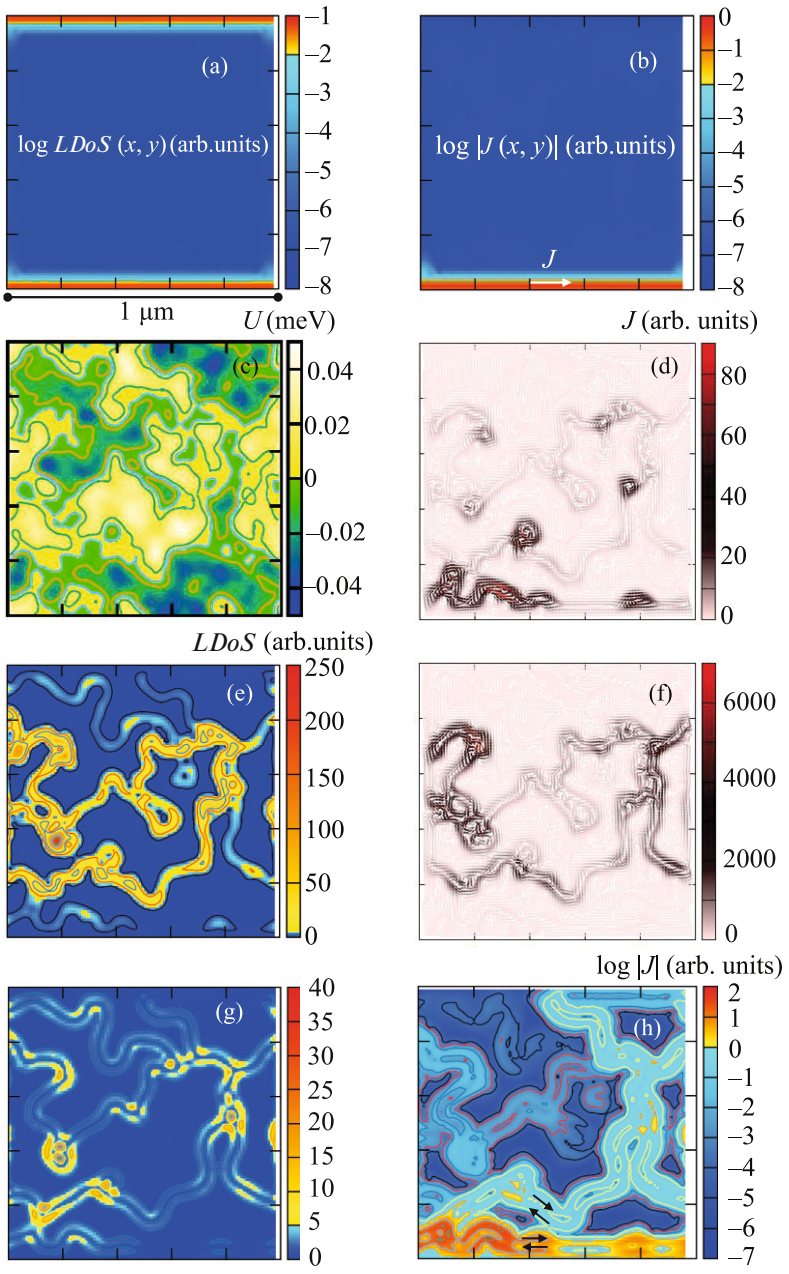

Fig. 4. (Color online) (a, e, g) Patterns of the local density of states and (b, d, f, h) nonequilibrium current in the scattering region. (a, b) Case of the deepest dip of the density of states in Fig. 2a ($n = 2eB/h$, $E_F = \hbar\omega_c$, $G = 2e^2/h$): (b) the usual edge state with the unidirectional current in the direction indicated by the arrow. (c) Effective potential $U(x, y)$ used to plot Figs. 2 and 3. (e) Example of increased *LDoS* lines running along the $U(x, y) = 0$ contours for states near the center of the lower Landau band with $E_F \approx \hbar\omega_c/2$ and $G = 0.7 \times 2e^2/h$. (d, f) Examples of high current density lines J running in opposite directions along the $U(x, y) = 0$ contours. (d) Case $G = 0.99 \times 2e^2/h$ at $n = 4.68 \times 10^{10}$ cm^{-2} corresponding to the narrow peak in Fig. 3. (f) Case $G = 0.084 \times 2e^2/h$ at $n = 5.05 \times 10^{10}$ cm^{-2} corresponding to the narrow dip. (g, h) State near the center of the second Landau band with $E_F \approx 3\hbar\omega_c/2$ and $G = 1.98 \times 2e^2/h$. Double lines of increased *LDoS* and double lines of opposite currents, indicated by arrows, run along the $U(x, y) = 0$ contours.

Figs. 4d and 4f, consist of two countercurrents. It is shown in the supplementary materials that similar countercurrents exist at the edge of structures, both at a stronger disorder and in the absence of disorder. They are caused by the rapid motion of a particle around the circle whose center slowly drifts. The edge

states appear in the form of countercurrents when the electrons populate approximately half of the Landau level (the drift velocity is close to zero) and are then transformed to unidirectional currents as the Landau level becomes almost fully populated (the drift velocity is high). The supplementary materials also show that narrow peaks at the edges (tails) of the Landau bands correspond to localized states in the form of ring currents that coexist with the edge current. Together with Figs. 2–4, this refines the predictions of the penetration of quantum plateaus R_{xy} into the region of localized states [3, 8].

We tested the stability of the conductance plateau under the variation of B from 1 to 3 T, change in the sample size from 1 to 3 μm, and variation of the potential parameters. If disorder was kept long-range and less than $\hbar\omega_c$ in magnitude, the strict plateaus of $G(n)$ deeply penetrated into the Landau bands. However, this effect disappeared at a fixed B value when long-range disorder was replaced by short-range one with the conservation of δU_{rms}. Finally, as shown in the supplementary materials, the increase in the channel width to 3 μm in the absence of disorder sharply narrows the quantized conductance plateaus and, therefore, destroys the QHE.

To summarize, at weak long-range disorder, the fine structure of the density of states in the quantum Hall effect has been numerically studied. In the central part of the Landau band, one-particle currents flow along the zero-potential contours in two opposite directions, which is associated with the slow drift of the electron. At the edges of the Landau band, the circular currents of the localized states inside the sample coexist with the edge currents at the sample boundaries. The quasiperiodic oscillations in the density of state correspond to the addition of two electrons to the scattering region. The widths of the conductance plateau and transition regions agree with the measurements.

ACKNOWLEDGMENTS

We are grateful to A.R. Hamilton, A.A. Bykov, Z.D. Kvon, G.M. Min'kov, D.G. Polyakov, and I.V. Gornyi for the discussion. Computing resources of the Interdepartmental Supercomputer Center of the Russian Academy of Sciences were used.

FUNDING

This work was supported by the Russian Science Foundation (project no. 19-72-30023).

REFERENCES

1. K. von Klitzing, G. Dorda, and M. Pepper, Phys. Rev. Lett. **45**, 494 (1980).
2. D. C. Tsui, H. L. Stormer, and A. C. Gossard, Phys. Rev. Lett. **48**, 1559 (1982).
3. H. Aoki, Rep. Prog. Phys. **50**, 655 (1987).
4. I. V. Kukushkin and V. B. Timofeev, Adv. Phys. **45**, 147 (1996).
5. V. T. Dolgopolov, Phys. Usp. **57**, 105 (2014).
6. M. J. Manfra, Ann. Rev. Condens. Matter Phys. **5**, 347 (2014).
7. H. Levine, S. Libby, and A. M. M. Pruisken, Phys. Rev. Lett. **51**, 1915 (1983).
8. K. Shizuya, Phys. Rev. Lett. **73**, 2907 (1994).
9. A. L. Efros, F. G. Pikus, and V. G. Burnett, Phys. Rev. B **47**, 2233 (1993).
10. K. Hashimoto, C. Sohrmann, J. Wiebe, T. Inaoka, F. Meier, Y. Hirayama, R. A. Römer, R. Wiesendanger, and M. Morgenstern, Phys. Rev. Lett. **101**, 256802 (2008).
11. J. R. Bindel, J. Ulrich, M. Liebmann, and M. Morgenstern, Phys. Rev. Lett. **118**, 016803 (2017).
12. D. B. Chklovskii, B. I. Shklovskii, and L. I. Glazman, Phys. Rev. B **46**, 4026 (1992).
13. J. Weis and K. von Klitzing, Phil. Trans. R. Soc. A **369**, 3954 (2011).
14. E. Brezin, D. J. Gross, and C. Itzykson, Nucl. Phys. B **235**, 24 (1984).
15. I. S. Burmistrov and M. A. Skvortsov, JETP Lett. **78**, 156 (2003).
16. J. Oswald and R. A. Römer, Phys. Rev. B **96**, 125128 (2017).
17. W. Zhu and D. N. Sheng, Phys. Rev. Lett. **123**, 056804 (2019).
18. S. Ilani, J. Martin, E. Teitelbaum, J. H. Smet, D. Mahalu, V. Umansky, and A. Yacoby, Nature (London, U.K.) **427**, 328 (2004).
19. O. E. Dial, R. C. Ashoori, L. N. Pfeiffer, and K. W. West, Nature (London, U.K.) **448**, 176 (2007).
20. M. Sammon, M. A. Zudov, and B. I. Shklovskii, Phys. Rev. Mater. **2**, 064604 (2018).
21. J. Nakamura, S. Fallahi, H. Sahasrabudhe, R. Rahman, S. Liang, G. C. Gardner, and M. J. Manfra, Nat. Phys. **15**, 563 (2019).
22. Z. D. Kvon, E. B. Ol'shanestkii, M. I. Katkov, A. E. Plotnikov, A. I. Toropov, N. T. Moshegov, M. Cassé, and J. C. Portal, Semiconductors **33**, 1238 (1999).
23. O. Couturaud, S. Bonifacie, B. Jouault, D. Mailly, A. Raymond, and C. Chaubet, Phys. Rev. B **80**, 033304 (2009).
24. N. Pascher, C. Rössler, T. Ihn, K. Ensslin, C. Reichl, and W. Wegscheider, Phys. Rev. X **4**, 011014 (2014).
25. X. Du, I. Skachko, F. Duerr, A. Luican, and E. Y. Andrei, Nature (London, U.K.) **462**, 192 (2009).
26. A. Grivnin, H. Inoue, Y. Ronen, Y. Baum, M. Heiblum, V. Umansky, and D. Mahalu, Phys. Rev. Lett. **113**, 266803 (2014).

27. S. Datta, *Electronic Transport in Mesoscopic Systems* (Cambridge Univ. Press, Cambridge, UK, 1997).

28. A. Cresti, R. Farchioni, G. Grosso, and G. P. Parravicini, Phys. Rev. B **68**, 075306 (2003).

29. O. A. Tkachenko, V. A. Tkachenko, Z. D. Kvon, A. L. Aseev, and J.-C. Portal, Nanotechnology **23**, 095202 (2012).

30. O. A. Tkachenko and V. A. Tkachenko, JETP Lett. **99**, 204 (2014).

31. O. A. Tkachenko, V. A. Tkachenko, I. S. Terekhov, and O. P. Sushkov, 2D Mater. **2**, 014010 (2015).

32. O. Tkachenko, V. Tkachenko, Z. Kvon, D. Sheglov, and A. Aseev, in *Advances in Semiconductor Nanostructures, Growth, Characterization, Properties and Applications,* Ed. by A. Latyshev, A. Dvurechenskii, and A. Aseev (Elsevier, Amsterdam, 2017), p. 131.

33. O. A. Tkachenko, D. G. Baksheev, V. A. Tkachenko, and O. P. Sushkov, in *Proceedings of the International Conference on Actual Problems of Computational and Applied Mathematics* (Novosib. Nats. Issled. Univ., Novosibirsk, 2019), pp. 509, 515.

Translated by L. Mosina